19th Australasian Fluid Mechanics Conference
Melbourne, Australia
8-11 December 2014

Investigation into the Effect of Vortex-Induced Vibrations on the Power-Output of a Pitching Cylinder Wave Energy Converter

A.W. Heath, and B. Stappenbelt

School of Mechanical, Materials and Mechatronics Engineering
University of Wollongong, Wollongong, New South Wales 2522, Australia

Abstract

The aim of the present investigation was to examine the question of whether the introduction of cross-flow vortex-induced vibration (VIV) of point absorber wave energy extraction devices is detrimental or beneficial to power take-off (PTO) efficiency. The dynamic drag amplification experienced by a circular cylinder undergoing cross-flow vortex-induced vibration is well documented for both the steady flow and oscillatory flow cases. The dynamic drag amplification experienced by a cylinder undergoing VIV in a wave environment indicates that there are potential benefits in allowing a drag dominated wave energy device to simultaneously experience cross-flow VIV. Experiments were conducted with a pivoted cylinder wave energy convertor to examine the power output of the system with and without cross-flow VIV over a range of wave amplitudes and frequencies. Near the optimal power take-off damping for the wave energy device, no consistent improvement in power take-off was observed with the introduction of VIV motions. A small improvement was noted at PTO damping levels higher than the optimal value.

Introduction

Wave energy from the ocean environment has long been considered a viable source for generating power [1, 3, 5]. A wave energy convertor (WEC) is a mechanical device which converts the energy in ocean waves into a more useful form, for example pressure or electrical [1, 3, 7]. Due to the hostile nature of the ocean environment, many issues must be overcome to ensure survivability of the WEC [2]. These increases capital and operational expenditure and hence the cost per kWhr of energy produced. To improve WEC economic viability relative to traditional fossil fuel based power plants, effective means of reducing capital cost or increasing the efficiency of power output must be developed.

This paper examines a novel idea for increasing the efficiency of a WEC through the use of cross-flow vortex induced vibration (VIV). VIV are a class of flow-induced vibration caused by the shedding of vortices as fluid passes a bluff object. As the fluid flows around the object, shear in the boundary layer generates vorticity. This vorticity coalesces to form vortices in the object's wake. As the vortices are shed from the object, pressure fluctuations are produced. These pressure fluctuations cause the object to vibrate if it is elastically restrained [6, 9, 10]. Objects undergoing VIV will experience greater drag forces compared to that of a still object [4]. In a wave environment the equation governing the relationship between static and dynamic drag coefficients is

$$C_D = C_0\left(1 + \frac{a}{D}\right). \quad (1)$$

where C_D represents the dynamic drag coefficient, C_0 is the static drag coefficient, a is the amplitude of the vibrations and D is the relative diameter of the object.

Generally when designing offshore structures, VIV is avoided [8]. In the present case, where the desired outcome is power production, the increased drag created by the introduction of VIV is sought for its potential to increase device efficiency. The WEC examined in the present study was a simple point absorber, pitching cylinder with the addition of a roll degree of freedom. The cylinder roll natural frequency was tuned to excite VIV at the peak water particle velocities induced by the passing waves.

Methodology

The experimental investigation conducted examined the power output of a pitching cylinder WEC. The device was tested in two configurations; one configuration where the cylinder was fixed in the roll degree of freedom, permitting only wave-induced pitching motions, and the other allowed for movement of the cylinder in the roll degree of freedom, allowing cross-flow VIV to occur. Both configurations were tested under a range of wave heights, frequencies and power take-off damping ratios.

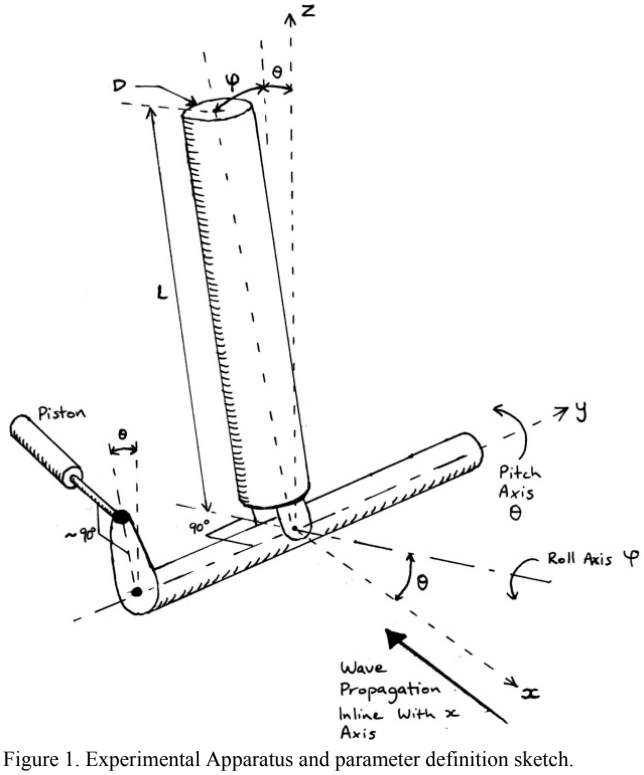

Figure 1. Experimental Apparatus and parameter definition sketch.

Power take-off was simulated using a piston damper. The level of damping was controlled by two one-way restricting valves. To measure the damping moment a load cell was placed behind the piston to measure the damper pitching moment. Two magnetic encoders were used to measure the angular position of the cylinder in the pitch and roll axis. The encoders had 9 bit resolution (i.e. 512 steps per revolution).

Figure 1 illustrates the configuration of the testing apparatus and acts as a parameter definition sketch. Table 1 lists the related experimental parameter values and ranges.

Parameter	Value/Range
θ - Pitch Angle	-30° to 30°
φ - Roll Angle	-30° to 30°
D - Cylinder Diameter	0.0825 m
Aspect Ratio - D/L	0.143
Damping Ratio - $b/b_{critical}$	0 – 4.5
m - Mass	1.692 kg
I - Inertia	0.262 kg.m^2
f_n - Still Water Natural Frequency	0.267 Hz
KC - Keulegan Carpenter Number	4.0 – 7.5
Re - Reynolds Number	7500 - 33000

Table 1. Experimental parameter values and ranges.

Some hysteresis was present in the torque-angular velocity behaviour of the piston. An equivalent linear damping coefficient was therefore defined by energy equivalence, equating the experimentally measured power output to the theoretical power output with linear damping as

$$\oint b\left(\frac{d\theta}{dt}\right)^2 dt = \oint \tau \frac{d\theta}{dt} dt. \qquad (2)$$

This yields a representative linear damping value of

$$b = \frac{\oint \tau \frac{d\theta}{dt} dt}{\oint \left(\frac{d\theta}{dt}\right)^2 dt}. \qquad (3)$$

In the equations above b is the linear damping coefficient and τ is the damping torque applied by the piston.

The wave energy conversion device was mounted to a frame and submerged in a 32.5m long, 1x1m cross-section wave tank. The wave maker was used to produce a range of waves at different frequencies and amplitudes. These waves were characterised according to their free surface Keulegan Carpenter ($KC = 2\pi a/D$) and Reynolds Numbers ($Re = \omega a D/\nu$). The generated waves were categorised into ten distinct KC and Re groupings. Table 2 summarises these, including the variation present within each group.

Grouping	KC	Log_{10}(Re)
1	4.4 ± 0.137	3.9 ± 0.017
2	4.8 ± 0.128	4.0 ± 0.013
3	5.1 ± 0.164	4.1 ± 0.013
4	5.1 ± 0.140	4.2 ± 0.011
5	5.2 ± 0.070	4.4 ± 0.006
6	6.4 ± 0.202	4.2 ± 0.014
7	6.3 ± 0.157	4.3 ± 0.010
8	6.4 ± 0.105	4.4 ± 0.008
9	7.2 ± 0.193	4.4 ± 0.012
10	7.3 ± 0.130	4.5 ± 0.008

Table 2. Experimental testing wave parameter groupings (±1 SD).

Results and Discussion

Figures 2 and 3 show data from the optimally damped tests of experimental grouping 1 (i.e. KC=4.4 and Re=7.9x10^3). Figure 2 shows data from the non cross-flow VIV configuration and figure 3 shows data from the with cross-flow VIV configuration.

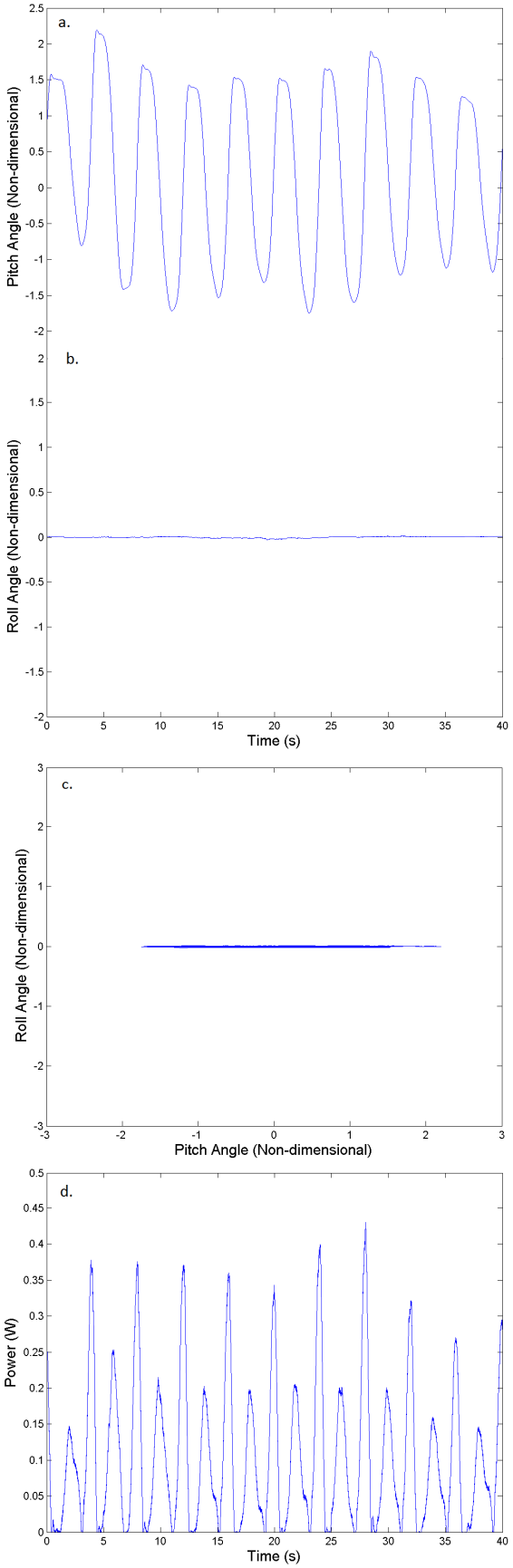

Figure 2. Results from the non cross-flowVIV configuration, optimal damping test, KC = 4.4, Re = 7.9x10^3 (grouping 1); a) time series of the pitch angle of the cylinder, b) time series of the roll angle of the cylinder, c) cylinder trajectory plot, and d) time series of the power output.

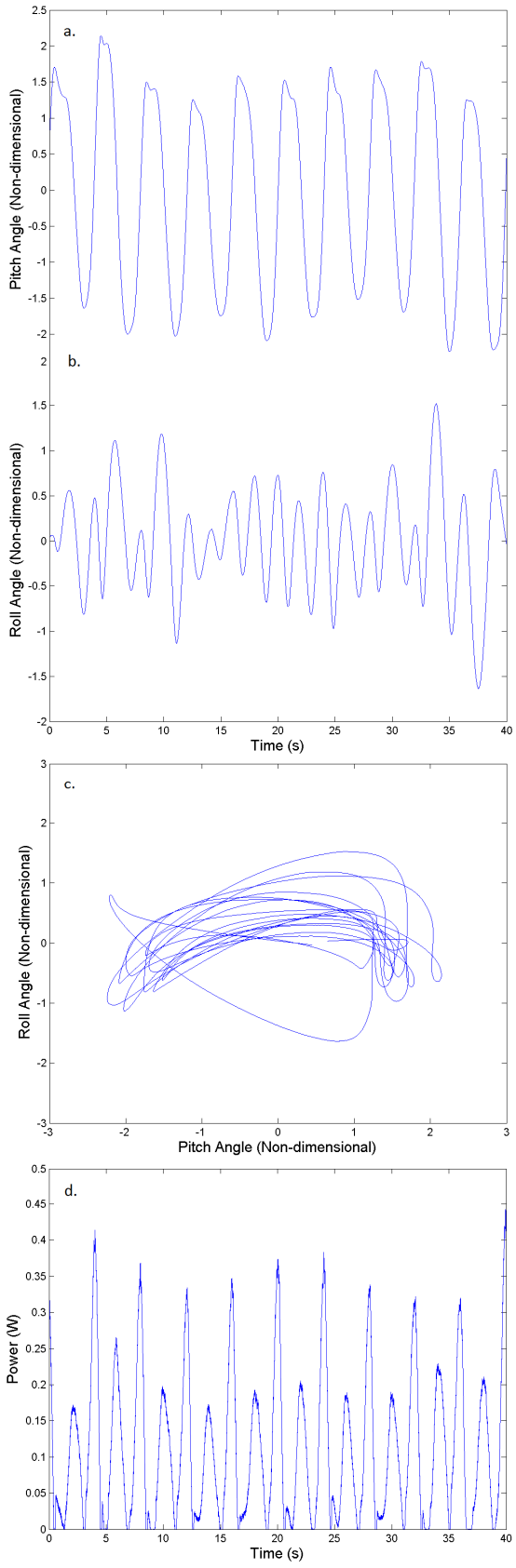

Figure 3. Results from the with cross-flow VIV configuration, optimal damping test, KC = 4.4, Re = 7.9X10^3 (grouping 1); a) time series of the pitch angle of the cylinder, b) time series of the roll angle of the cylinder, c) cylinder trajectory plot, and d) time series of the power output.

Figure 2a shows the pitch angle of the device over ten wave cycles. The amplitude varies slightly over the duration of the ten wave cycles, and the centre point appears to drift around the zero mark. Figure 2b shows no movement of in the roll degree of freedom indicating no cross-flow VIV is occurring. Figure 2c shows the trajectory of the cylinder restrained to one degree of freedom (i.e. pitch). Figure 2d shows the power output with time. The alternating peaks indicate the forward and backward stroke of the cylinder. The difference in peak heights is at least in part explained by the hysteresis in the damping mechanism employed in the present experimental study.

Figure 3a illustrates the pitch angle of the cylinder over ten wave cycles and has similar form and magnitude to that of figure 2a. Figure 3b shows the roll angle of the device over ten wave cycles representing the cross-flow VIV motion of the cylinder. The cross-flow VIV observed was often irregular, with periods of low and high amplitude oscillations. These fluctuations would be expected to coincide with the variation in wave water particle velocities however, when compared to the power output of the device in figure 3d, there is no clear correlation.

Figure 3c again illustrates the trajectory of the cylinder over ten wave periods. Cross-flow VIV was clearly present with two vortex-induced vibration oscillations occurring every wave cycle. This creates the "C" shaped trajectory. For higher wave frequencies, and hence Reynolds Numbers, only one oscillation occurred for each wave cycle. An example of such a trajectory plot is presented in figure 4 for KC = 7.3, Re = 3.2x10^4.

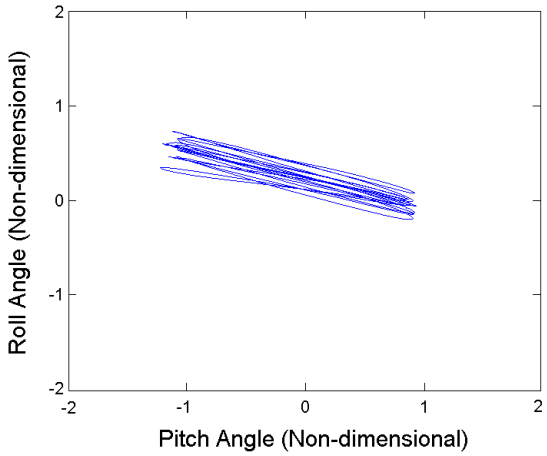

Figure 4. Trace plot from the VIV configuration, medium level damping test, KC = 7.3, Re = 3.2x10^4 (grouping 10).

The sample time series of figures 2 and 3 typify the WEC device response observed at or near optimal PTO damping conditions across the KC and Re range tested. There is very little difference in the pitch response and instantaneous power output with or without the cross-flow vortex-induced vibration. When the capture width is non-dimensionalised by the physical width of the device (i.e. the diameter D), then this results in essentially no difference in capture width for the two tested configurations. When the cross-flow motions are included in the device width governing the available power resource, then the cross-flow VIV configuration results in relatively lower capture width values.

Figures 5, 6, and 7, present the capture width (non-dimensionalised by the device diameter, D) as a function of the PTO damping ratio for each test conducted in groupings 1, 5 and 10 respectively. Each plot clearly demonstrates that an optimal PTO damping does exist as expected. The peak efficiency appears to occur at higher PTO damping with increasing KC number. The magnitude of the peak capture width however decreases with increasing KC.

It is clear there is only a slight difference in the peak capture widths of the VIV and non-VIV configurations. The

configuration with greatest capture width varies from one experimental group to another. The optimal damping appears to occur close to the same position for both configurations across all experimental groups. The VIV configuration occasionally allowed for a greater capture width when experiencing damping conditions above the optimal.

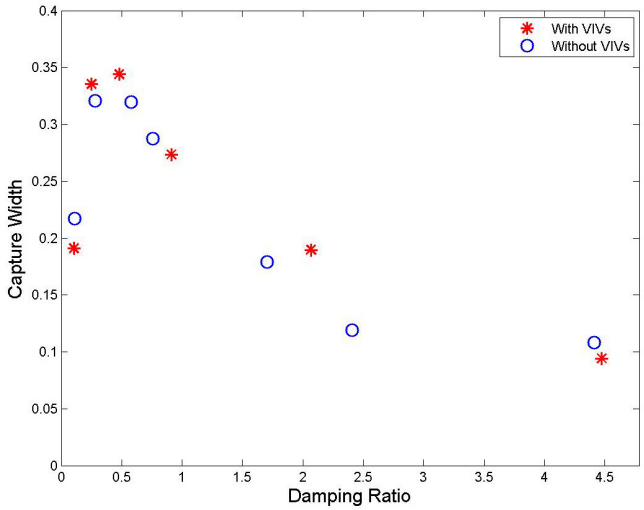

Figure 5. Capture width as a function of PTO damping ratio for experimental grouping 1.

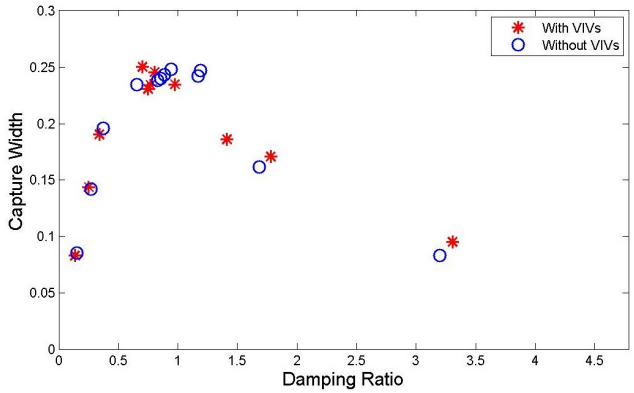

Figure 6. Capture width as a function of PTO damping ratio for experimental grouping 5.

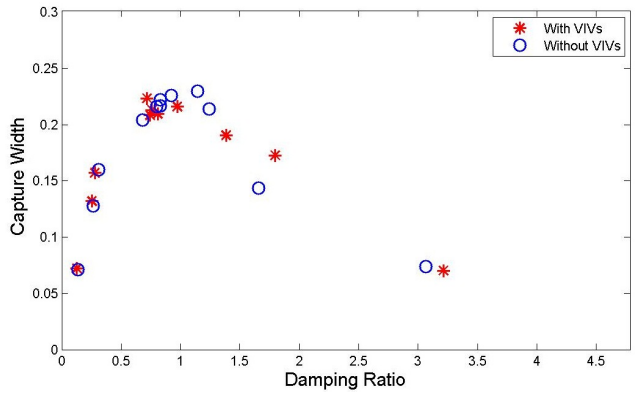

Figure 7. Capture width as a function of PTO damping ratio for experimental grouping 10.

Conclusions

A summary of the optimal damping and corresponding peak capture widths has been provided in figure 8. The peak capture width of the each configuration in each experimental group was determined and plotted against its respective Reynolds number. Groupings with very similar Keulegan-Carpenter numbers have been joined by solid or dashed lines. Solid lines represent the non cross-flow VIV configuration and dashed lines represent the with cross-flow VIV configuration. A discernable dependency of the peak capture width of the WEC device on the Reynolds number is visible from this plot.

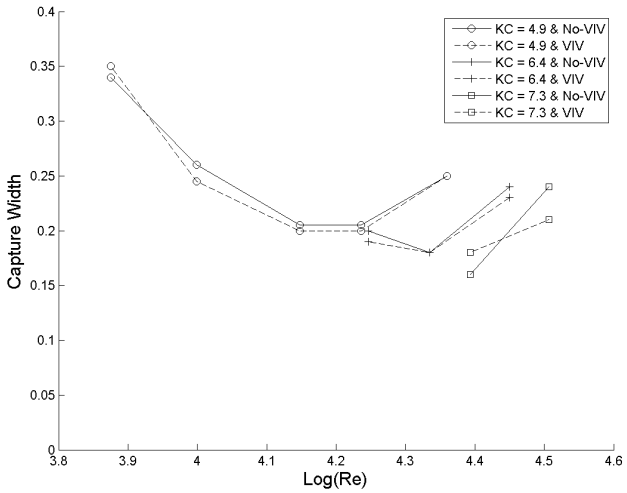

Figure 8. Peak capture width with respect to Reynolds Number.

The maximum capture width results of figure 8 again show that at optimal damping there is no significant increase in PTO efficiency of the pitching cylinder WEC with cross-flow VIV present for the range of Keulegan Carpenter and Reynolds numbers tested. At PTO damping above optimal however, there does appear to be a small improvement in capture width. Further testing is required to verify this and ascertain the extent of this effect at higher and lower Keulegan Carpenter numbers than those covered in the present investigation.

References

[1] Al´ement et al. Wave energy in Europe: current status and perspectives. *Renewable and Sustainable Energy Reviews* **6**, 2002, 405–431.

[2] Dalrymple R.A. and Dean R.G. *Water Wave Mechanics for Engineers and Scientists*. World Scientific Publishing Co. Pte. Ltd, 5 Toh Tuck Link, Singapore, 1991.

[3] Drew B., Plummer A.R., and Sahinkaya M.N. A review of wave energy converter technology. *Journal of Power and Energy* **223**, 2009, 887–902.

[4] Det Norske Veritas, *Environmental Conditions and Environmental Loads*, Høvik, Norway, 2007.

[5] Falnes J. A review of wave-energy extraction. *Marine Structures* **20**, 2007, 185–201.

[6] Fredsøe J. and Sumer B.M. *Hydrodynamics Around Cylindrical Structures*. World Scientific Publishing, Singapore, 1997.

[7] Fujita R.M. and Pelc R. Renewable energy from the ocean. *Marine Policy* **26**, 2002, 471–479.

[8] Gao Y., Sun L., and Zong Z. Numerical prediction of fatigue damage in steel catenary riser due to vortex-induced vibration. *Journal of Hydrodynamics* **23**, 2011, 154–163.

[9] Govardhan R. and Williamson C.H.K. A brief review of recent results in vortex-induced vibrations. *Journal of Wind Engineering and Industrial Aerodynamics* **96**, 2008, 713–735.

[10] Jauvtis N. and Williamson C.H.K.. Vortex-induced vibration of a cylinder with two degrees of freedom. *Journal of Fluids and Structures* **17**, 2003, 1035–1042.